

Antenna-Impregnated Fabrics for Recumbent Height Measurement on the Go

Keren Zhu, Lisa Militello, and Asimina Kiourti, *Member, IEEE*

Abstract A novel class of antenna-impregnated fabrics is proposed for wireless and unobtrusive height measurement on the go. Contrary to conventional infantometer and stadiometer technologies that restrict height monitoring to sporadic intervals, this technology brings forward regular height monitoring with minimum impact to the individual's activity. The proposed fabrics consist of multiple dipole antennas placed at known distances from each other. When a subject lies upon the fabric, he/she detunes the underlying antennas, inducing losses in the associated wireless transmission paths. Therefore, the subject's height can be calculated by identifying the two antennas with degraded transmission coefficients at the starting (head) and ending (feet) points. For validation, a proof-of-concept 52cm×43cm fabric operating at 915 MHz is designed, fabricated and tested. Simulation and *in-vitro* measurement results demonstrate the feasibility of retrieving the length of a 16-cm-long phantom, regardless of its exact location upon the fabric. Concurrently, the proposed fabric is shown to conform to the Federal Communication Commission guidelines for the Specific Absorption Rate (SAR). This technology can eventually be integrated into baby cribs, bed sheets or rollable mats to provide early detection/monitoring of Turner syndrome, Crohn's disease, short stature, Celiac disease, growth hormone deficiency, and obesity, among others.

Keywords — Dipole antennas, flexible antennas, height measurement, transmission coefficient, wireless telemetry.

I. INTRODUCTION¹

RECENT studies indicate an increasing need for monitoring human height on a regular basis, particularly for assessing children's health in their early years [1], [2]. Growth monitoring may help to early identify conditions that include, but are not limited to, Turner syndrome [3], Crohn's disease [4], growth hormone deficiency (GHD) [4], short stature [5], Celiac disease [6], and obesity [7]. Notably, failure to identify/treat these conditions at an early stage is known to increase the risk for several other health implications in future (short stature [8], [9], high body mass index [10], low glucose tolerance [10], distress [10], osteoporotic bone loss [11], etc.).

Existing practices for monitoring children's height rely on manual, time-consuming, inefficient, and rather cumbersome measurements. As an example, the standard height measurement process for children under 24 months entails the use of an infantometer [12]. The latter requires two anthropometrists to record the height of a child: one keeps the child's head snugly so that it touches a fixed

vertical plank, while the other presses over the knees, places a second moveable plank at the end of the feet, and records the height [13]. At older ages, height is typically measured using a tape measure or a stadiometer. Though straightforward and simple, these methods are still time-consuming and prone to measurement errors. The American Academy of Pediatrics recommends monitoring children's height per the periodicity schedule reported in [14]. Such data should, eventually, be compared with the World Health Organization growth standards (0-2 years old) or the Centers for Disease Control and Prevention growth charts (> 2 years old) to identify abnormal growth [15]. Depending on the diagnosis, a treatment plan is finally employed that should, in turn, involve regular (per case) height monitoring (e.g., at least 4 times per year for GHD therapy) [16]. However, in practice, the proportion of well-child visits declines with age, and is far less for uninsured children [17]. Thus, current approaches to regularly monitor height are inefficient and have the potential to be improved with technological advances.

An automated way of unobtrusively monitoring height on a regular basis would offer unprecedented opportunities in monitoring children's growth and providing early detection/prevention of related disorders [18]. With this in mind, we are proposing a new class of antenna-impregnated fabrics for wireless recumbent height monitoring on the go. In brief, the proposed fabrics consist of multiple dipole antennas placed at known intervals/distances from each other. The two antennas placed at the ends of the fabric are

Manuscript received November 30, 2017, revised January 26, 2018 and February 21, 2018. This work was supported in part by The Innovation Studio.

K. Zhu and A. Kiourti are with the ElectroScience Laboratory, Department of Electrical and Computer Engineering, The Ohio State University, Columbus, OH 43212, USA (e-mails: zhu.1266@osu.edu, kiourti.1@osu.edu).

L. Militello is with the College of Nursing, The Ohio State University, Columbus, OH, 43210, USA (e-mail: militello.14@osu.edu).

transmitting (one at a time), while the rest are receiving. When a subject is lying upon the fabric, he/she detunes the underlying antennas, inducing losses in the associated wireless transmission paths. Therefore, the subject's height can be calculated by identifying the two antennas with degraded transmission coefficients at the starting point (head) and ending point (feet) of the human body, respectively. In the past, we have explored the use of adjacent dipole antennas printed upon flexible substrates (fabrics, polymers, etc.) for deep-tissue imaging applications [19], [20]. However, this is the first time that unobtrusive and wireless height measurement is explored via the use of antenna-impregnated fabrics.

In this paper, we present a proof-of-concept demonstration of the proposed antenna-impregnated fabrics for recumbent height monitoring. The developed fabric occupies $52\text{ cm} \times 43\text{ cm}$, and consists of 16 dipole antennas placed at 2 cm distance from each other. The latter implies a 2-cm-resolution in retrieving the height/length of a subject/phantom placed upon the fabric. Of course, denser dipole placement can be implemented in future to realize higher resolution. For example, $\sim 1\text{-cm}$ -resolution, that is within the error range of currently used height monitoring techniques for children [21], can be achieved just by doubling the number of dipole antennas. In turn, this implies a trade-off between computation time and resolution, to be optimized per the application in hand. For wireless operation, the 915 MHz band is selected, as: a) it is an Industrial, Scientific, and Medical (ISM) applications band [22], and b) its associated wavelength ensures a reasonable dipole length for the intended application (i.e., the antennas should be long enough to be covered by the overlying phantom, while still ensuring a reasonable size for the overall fabric). Finite Element (FE) simulations and *in-vitro* measurement results demonstrate the capability of the proposed fabric to accurately detect the length of a 16-cm-long tissue-emulating phantom placed upon its surface. Notably, this recumbent height detection capability is not limited in any way by the exact placement of the phantom upon the mat (e.g., phantom placed in the middle of the fabric vs. phantom placed towards the edge of the fabric). Even more importantly, the proposed concept is scalable to any desired fabric size and any desired accuracy (viz. inter-antenna distance), per the application requirements. Specific absorption rate (SAR) performance and conformance to Federal Communications Commission (FCC) guidelines for human safety [23] are also taken into consideration. To our knowledge, this is the first time that a wireless and unobtrusive solution is proposed for height monitoring on the go.

Expectedly, the proposed antenna-impregnated fabrics can be integrated into several usage scenarios for recumbent height monitoring. Examples include: a) bed sheets that unobtrusively collect digital height data for children; b) smart baby cribs that monitor baby growth on a continuous basis; c) rollable mats that can be hang on the wall or placed upon the floor to measure the height of the overlying

subject, etc. For young children, the process of maintaining a straight posture, as required for height measurement via the proposed technique, is straightforward. For infants, assistance will still be needed to some extent. However, instead of two anthropometrists currently needed to operate an infantometer, only one person will now be required, while the measurement can further be performed inside a home rather than a clinical environment. In another envisioned scenario, the fabrics could collect measurements throughout the infant's sleep, and eventually record height as the highest value measured, e.g., overnight (assuming that the infant changes postures during sleep, the longest dimension recorded would be that of the infant in straight position). The collected data could eventually be wirelessly transmitted (e.g., through Bluetooth) to a nearby cell phone or other Personal Digital Assistant (PDA) device. Overall, the proposed design brings forward transformational opportunities for monitoring human growth, promising to reform existing healthcare monitoring practices and promoting a better quality of life for individuals.

II. METHODS AND PROCEDURES

A. Operation Principle

The operation principle of the proposed antenna-impregnated fabrics is summarized in Fig. 1. As seen in Fig. 1(a), the fabric consists of multiple dipole antennas (N in number) placed at known intervals/distances from each other (d). In order to enlarge the surface area where the subject may lie upon the fabric for recumbent height measurement, asymmetric feeds are selected for the antennas (i.e., one dipole arm is longer than the other). In addition, a ground plane is added underneath the fabric to avoid any disturbance from the per-case underlying surface (e.g., fabric lying upon a wooden vs. metal-based surface).

The two antennas at the opposite ends of the mat are transmitting (Tx), one at a time, while the rest are receiving (Rx). The 915-MHz-band is selected for this wireless transmission, as discussed above. When a subject/phantom is placed on top of the fabric, the former will detune the underlying antennas, inducing losses in the associated wireless transmission paths. Therefore, the subject's height (or, equivalently, the phantom's length) can be calculated by identifying the two antennas with degraded transmission coefficients at the starting point (head) and ending point (feet) of the human body, respectively.

As shown in Fig. 1(b), height measurement via the proposed antenna-impregnated fabrics is enabled via a four-step process:

- *Step 1: Front baseline sweep.* This sweep is performed without the presence of any subject/phantom upon the mat. In this case, antenna #1 is transmitting, while the rest (antennas #2 to #N) are receiving. In doing so, a set of front-scan baseline transmission coefficient values are obtained, viz. $|S_{2,1}|_b, |S_{3,1}|_b \dots |S_{N,1}|_b$.
- *Step 2: Back baseline sweep.* This sweep is again performed without the presence of any subject/phantom upon the mat. In this case, antenna #N is transmitting, while the rest (antennas #1 to #N-1) are receiving. In doing so, a

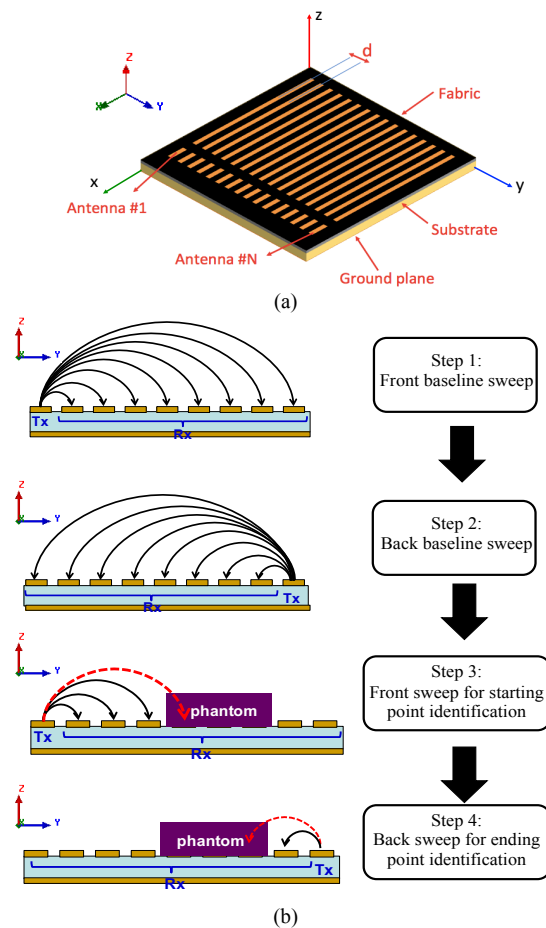


Fig. 1. Operation principle of the proposed antenna-impregnated fabrics: (a) design, and (b) four-step measurement process for deriving the length of the overlying phantom.

set of back-scan baseline transmission coefficient values are obtained, viz. $|S_{N-1,M}|_b, |S_{N-2,M}|_b, \dots, |S_{1,M}|_b$.

- **Step 3: Front sweep for starting point identification.** The subject/phantom is placed upon the mat, and the aim is to identify its starting point location. To do so, antenna #1 is transmitting, while the rest (antennas #2 to #N) are receiving. Sequential transmission coefficient measurements are obtained, starting with antenna #2 ($|S_{2,1}|$), and moving on up to antenna #I ($|S_{I,1}|$). Here, #I refers to the first antenna that exhibits a significantly lower transmission coefficient value as compared to its corresponding front baseline sweep value of Step 1. In our design, the target difference for the aforementioned transmission coefficient values is > 5 dB in absolute value. Antenna #I is identified as the starting point of the subject/phantom upon the fabric.

- **Step 4: Back sweep for ending point identification.** The subject/phantom is placed upon the mat, and the aim is to identify its ending point location. To do so, antenna #N is transmitting, while the rest (antennas #1 to #N-1) are receiving. Sequential transmission coefficient measurements are obtained, starting with antenna #N-1 ($|S_{N-1,M}|$), and moving on up to antenna #J ($|S_{J,M}|$, where $J > I$). Here, #J refers to the first antenna that exhibits a

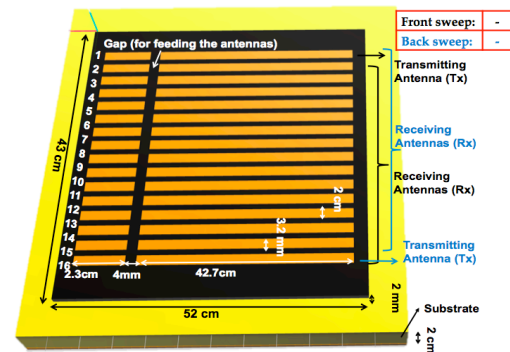


Fig. 2. Design parameters of the proposed proof-of-concept design.

significantly lower transmission coefficient value as compared to its corresponding back baseline sweep value of Step 2. Same as in Step 3, our target difference for the aforementioned transmission coefficient values is > 5 dB in absolute value. Antenna #J is identified as the ending point of the subject/phantom upon the fabric.

The height of the subject (or, equivalently, the length of the phantom) can eventually be calculated as:

$$Height = [(J - I) + 1] \times d \quad (1)$$

B. Simulation Set-Up and Proof-of-Concept Fabric Design

For validation, a proof-of-concept fabric was designed, fabricated and tested. As shown in Fig. 2, our proof-of-concept fabric occupied a footprint of 52 cm x 43 cm, and consisted of 16 dipole antennas placed at 2 cm intervals from each other. Felt ($\epsilon_r = 1.45$, $\sigma \approx 0$ S/m) and flexible foam ($\epsilon_r \approx 1$, $\sigma \approx 0$ S/m) were selected as the fabric and substrate materials, respectively. Thickness of the felt fabric was set equal to 2 mm to match the thickness of the corresponding material available in our lab.

The rest of the design parameters, viz. dipole dimensions and substrate thickness were optimized using Finite Element (FE) simulations in Ansys HFSS. The design goal was to concurrently achieve: a) reflection coefficient values of < -10 dB for all antennas at 915 MHz, and b) a difference of > 5 dB between $|S_{I,1}|$ and $|S_{I,1}|_b$, as well as between $|S_{J,M}|$ and $|S_{J,M}|_b$, defined in Section II.A. The latter requirement was determined via a series of simulations that considered various phantom shapes/sizes. For this proof-of-concept study, the phantom is emulated as a square-footprint box, occupying a surface area of 16 cm x 16 cm, and exhibiting properties equal to the average of human tissues at 915 MHz ($\epsilon_r = 56.8$, $\sigma = 1.07$ S/m) [23]. Such single-tissue canonical phantoms have extensively been employed in the literature to emulate the average properties of the human body [24] and head [25], among others. More accurate multi-layer and/or anatomical phantoms will be pursued in future. In an attempt to simulate a worst-case scenario, the phantom's thickness is selected to be equal to only 1 cm. Expectedly, thicker phantoms are anticipated to exhibit much more pronounced differences between the intended transmission coefficient values. The 0.5-mm gap between

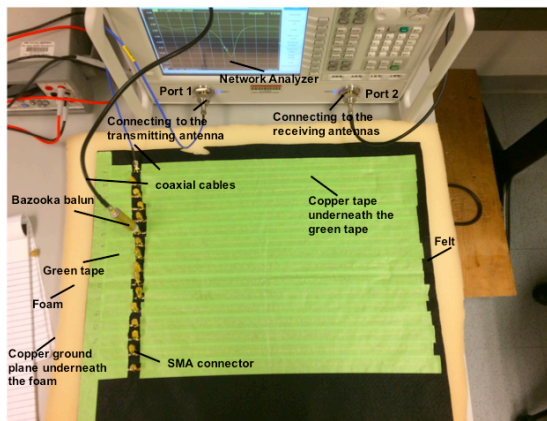


Fig. 3. Fabricated fabric prototype and *in-vitro* experimental set-up.

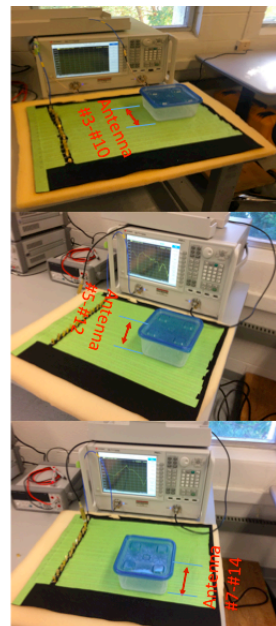
TABLE I
 AVERAGE-BODY PHANTOM RECIPE AT 915MHZ [23]

Ingredients	% by weight
Water	56.0
Salt (NaCl)	0.76
Sugar	41.76
HEC	1.21
Bactericide	0.27

the fabric and the phantom introduced by the container itself is negligible and can rather emulate the presence of clothing worn by the subject. Preliminary simulations for even thicker gaps have indicated no deterioration in the achieved performance. Perfect electric conductor boundaries were assigned to all metal surfaces, including the antennas and the ground plane. Radiation boundaries were set at a distance of $> \lambda/4$ away from the structure (free space wavelength at 915 MHz (λ) ≈ 32.7 cm, implying that $\lambda/4 \approx 8$ cm). The optimized design parameters of our proof of concept prototype are summarized in Fig. 2.

C. In-Vitro Measurement Set-Up

In-vitro measurements were conducted to validate the simulated design and performance. Our proof-of-concept antenna-impregnated fabric prototype is shown in Fig. 3, and was fabricated using the optimized dimensions of Fig. 2. Specifically, 2-mm-thick felt ($\epsilon_r = 1.45$, $\sigma \approx 0$ S/m) and 2-cm-thick foam ($\epsilon_r \approx 1$, $\sigma \approx 0$ S/m) were used to realize the fabric and substrate, respectively. For this proof-of-concept design, copper tape was used to realize the antennas and ground plane, respectively. As seen in Fig. 3, green tape, with properties similar to free-space, was used to secure the antennas upon the fabric and avoid potential delamination. In future, textile-based antennas could be directly embroidered upon the fabric [26]-[29]. Our prior work has demonstrated that E-textile prototypes exhibit the same RF performance as that of their copper equivalents [23]-[26]. As such, dipole embroidery via E-threads is anticipated to be a straightforward process, yet outside the scope of this specific work. Also, the fabric may in future be coated with breathable thermoplastic polyurethane [30], [31] to overcome potential issues associated with moisture trapping [32], [33]. The latter is anticipated to require only a minor fine-tuning of the antenna design so as to take the superstrate-coating into account.



SCENARIO A: Phantom placed at top of the fabric, covering dipoles #3 to #10

SCENARIO B: Phantom placed in the middle of the fabric, covering dipoles #5 to #12

SCENARIO C: Phantom placed at the end of the fabric, covering dipoles #7 to #14

Fig. 4. Measurement scenarios for retrieving the phantom length when placed at different locations upon the fabric.

Transmission coefficient measurements were obtained using a 2-port network analyzer connected to the corresponding dipole antennas via coaxial cables. The output power for the network analyzer was set to -30dBm (10 μ W). Port 1 of the network analyzer was connected to the transmitting antenna, while port 2 was connected to the receiving antennas one at a time, as shown in Fig. 3. For this proof-of-concept prototype, SMA connectors were soldered to each of the ports, and further connected to bazoooka baluns for enabling unbalanced operation. Loads of 50 Ω were connected to each of the “open” antenna ports to prevent them from re-radiating. A liquid phantom was prepared that emulated the average human body properties at 915 MHz ($\epsilon_r = 56.8$, $\sigma = 1.07$ S/m) [23]. The phantom consisted of water, salt, sugar, Hydroxyethyl Cellulose (HEC) and bactericide, as shown in Table I [23]. To accurately emulate the corresponding simulation scenario, the phantom occupied 16 cm \times 16 cm \times 1 cm (covering 8 antennas upon the fabric).

III. RESULTS

A. Proof-of-Concept Fabric Validation

To validate our design, we aimed at identifying the length of the phantom (i.e., 16 cm) when placed upon the developed proof-of-concept antenna-impregnated fabric. A key concern in this case is to ensure that the phantom’s length can be accurately retrieved regardless of its exact position upon the fabric. Along these lines, three scenarios were tested in both simulations and measurements. For Scenario A, the phantom was placed near the top of the fabric, blocking antennas #3 to #10 (see Fig. 4(a)). For Scenario B, the phantom was placed approximately in the middle of the fabric, blocking antennas #5 to #12 (see Fig. 4(b)). For Scenario C, the phantom was placed near the end of the fabric, blocking antennas #7 to #14 (see Fig. 4(c)).

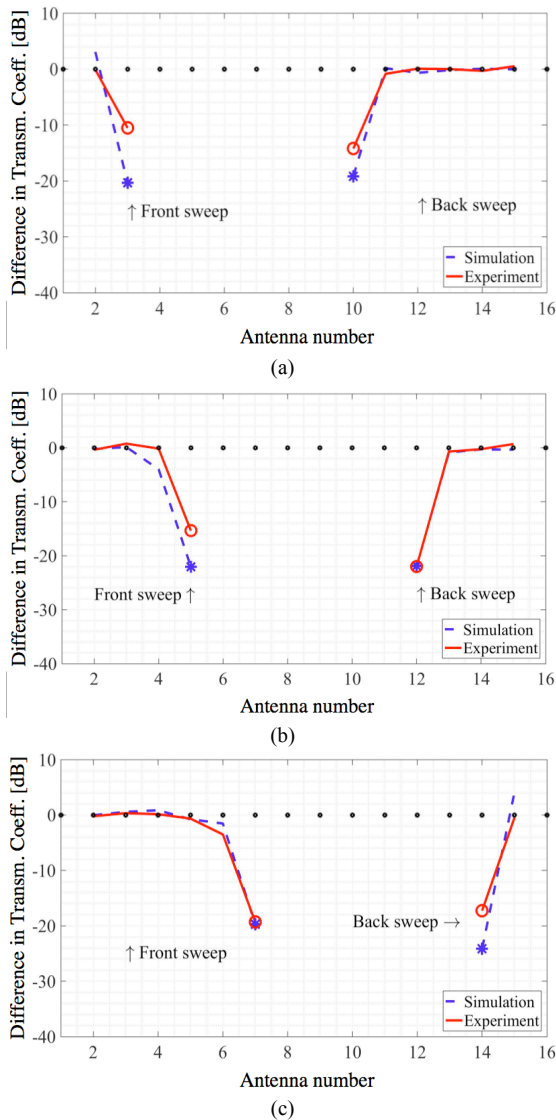


Fig. 5. Difference in transmission coefficients between the baseline measurements and the measurements with an overlying phantom: (a) phantom placed upon antennas #3-#10, (b) phantom placed upon antennas #5-#12, and (c) phantom placed upon antennas #7-#14.

Measurement and simulation results are super-imposed in Fig. 5 for all three scenarios of Fig. 4. Notably, insignificant discrepancies are observed between simulations (dotted lines) and *in-vitro* experimental results (solid lines). Specifically, Fig. 5 plots the difference in the transmission coefficient values between the baseline case vs. the case where the phantom lies upon the mat for both the front and back sweeps described in Section II. The starting and ending points of the phantom can be clearly identified by the antenna location in each sweep where the transmission coefficient exhibits a significant decrease. Specifically, as discussed in Section II, when the drop of the transmission coefficient vs. its corresponding baseline value is higher than 5 dB, then the starting and ending points of the phantom have been identified.

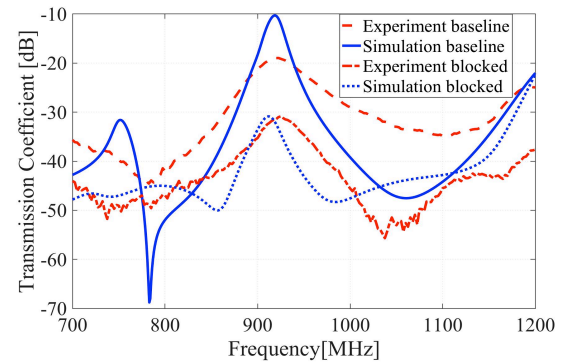


Fig. 6. Transmission coefficient frequency response for Scenario A, assuming that antenna #1 is transmitting and antenna #3 is receiving.

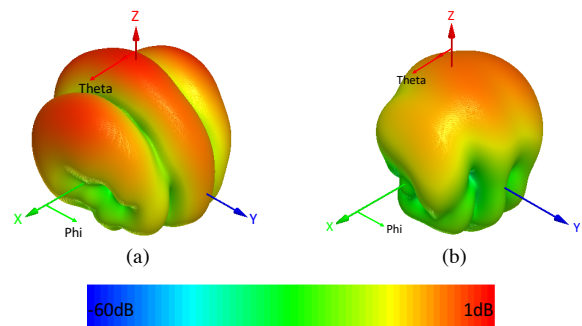


Fig. 7. Realized gain patterns exhibited by antenna #3 in Scenario A: a) without phantom, and b) with phantom lying upon the mat.

Indeed, for Scenario A, Fig. 5(a) indicates that the phantom extends between dipoles #3 and #10. As such, and based on Eq. (1), the length of the phantom is found to be equal to 16 cm, which is indeed the case. An example transmission coefficient frequency response is shown in Fig. 6. In this particular case, antenna #1 is transmitting, while antenna #3 is receiving. Both simulation and experimental results are shown for the case when no phantom lies upon the fabric vs. the case when a phantom covers antennas #3 to #10. Discrepancies between simulations and measurements may be attributed to fabrication errors and losses associated with the realistic measurement environment (green tape used to secure the antennas, surrounding objects in the testing space, etc.). The 3-D realized gain radiation patterns exhibited by antenna #3 in these two cases are shown in Fig. 7 (assuming the coordinate system defined in Fig. 1(a)). Similarly, for Scenario B, Fig. 5(b) indicates that the phantom extends between dipoles #5 and #12, while for Scenario C, Fig. 5(c) indicates that the phantom extends between dipoles #7 and #14. Thus, Eq. (1) again indicates that the correct phantom length of 16 cm is again retrieved. That is, in all cases, the fabric was able to detect the starting and ending points of the phantom, and, thus, retrieve its length. Even more importantly, the phantom length could be accurately retrieved regardless of its exact positioning upon the fabric. All aforementioned measurements were repeated at least 3 times, and height was accurately retrieved in all cases. Of

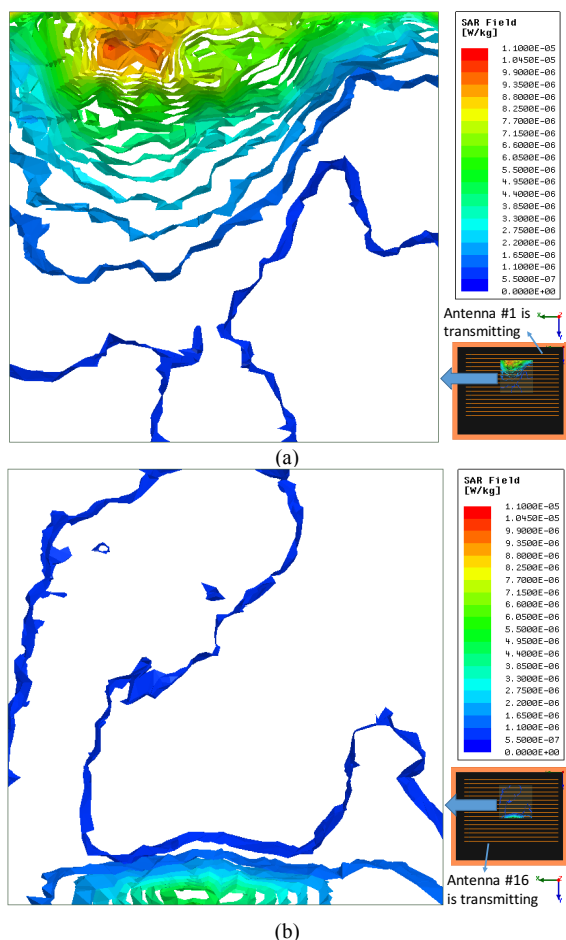


Fig. 8. SAR_{1g} distribution inside the phantom of Scenario A assuming an input power of 10 μ W: (a) antenna #1 is transmitting (front sweep) (b) antenna #16 is transmitting (back sweep).

course, the resolution was as high as 2 cm, as dictated by the employed antenna separation distance.

B. SAR Performance

As is well-known, the FCC safety guidelines for human exposure to electromagnetic fields limit the SAR averaged over any 1 gr of tissue to SAR_{1g} < 1.6 W/kg [23]. With this in mind, SAR simulations were performed in ANSYS HFSS to evaluate compliance of our proof-of-concept fabric design vs. the aforementioned guidelines.

To do so, the phantom mass density was set to 1.04 gr/cm³ [34], and the antenna input power was set to 10 μ W to match the corresponding power level used in Section III.A. Of course, the maximum allowable power levels are to be determined by FCC regulations, as will be discussed next. The maximum SAR_{1g} values recorded for all three scenarios of Fig. 4 are summarized in Table II. As an example, Fig. 8 plots the SAR_{1g} distribution within the phantom for an input power of 10 μ W. Both the front sweep (Fig. 7(a)) and back sweep (Fig. 7(b)) cases are provided, demonstrating, expectedly, higher SAR_{1g} values at the areas closer to the corresponding transmitting antennas. It is noted that even for Scenario B, where the middle-lying antennas are covered (#5-#12), the phantom was actually placed a bit off the symmetry axis, and lying closer to antenna #16. In turn, the maximum allowable input power

levels that still guarantee conformance with the FCC limitation are also given in Table II. It is worth noting that, though the FCC does not differentiate its standards based on child vs. adult exposure, the American Academy of Pediatrics [35] and the U.S. GAO [36] support their future reassessment for children. Indeed, children/infants are different than adults in terms of size and anatomy, and several studies have compared their associated RF exposure. For example, [37] concluded that cell phones generate higher SAR levels in children's heads, while [38] claimed that the effects of even the same dose on the developing brain of a child could be greater than adults. In any case, and as demonstrated in Section III.A, the proposed device can still operate at 10 μ W input power, implying $\sim 10^5$ times lower SAR_{1g} than that recommended by FCC.

TABLE II
SAR SIMULATION RESULTS

	Max. SAR _{1g} for an input power of 10 μ W [W/kg]		Max. allowable input power by FCC [W]	
	Tx: Ant. #1	Tx: Ant. #16	Tx: Ant. #1	Tx: Ant. #16
Scenario A	1.05 $\cdot 10^{-5}$	5.02 $\cdot 10^{-6}$	1.5 W	3.1 W
Scenario B	4.92 $\cdot 10^{-6}$	7.15 $\cdot 10^{-6}$	3.15 W	2.2 W
Scenario C	3.00 $\cdot 10^{-6}$	1.31 $\cdot 10^{-5}$	5.3 W	1.2 W

IV. CONCLUSION

A novel class of antenna-impregnated fabrics was presented for recumbent height monitoring on the go. The proposed fabrics consist of a multitude of dipole antennas placed next to each other at known distances. Height can be accurately derived by identifying the location of the detuned antennas when a subject/phantom lies upon the fabric. Proof-of-concept simulation and *in-vitro* measurement results for a 52 cm \times 43 cm fabric were in good agreement and were shown to accurately derive the length of a 16-cm tissue-emulating phantom. Even more importantly, results demonstrated that height can be retrieved regardless of the exact position of the phantom upon the fabric (e.g., phantom placed in the middle of the fabric vs. phantom placed towards the edge of the fabric). Concurrently, our design was shown to conform with the FCC standards for the SAR.

The proposed antenna-impregnated fabrics are scalable to any size and/or accuracy requirements, as enabled by the antenna number and intervals, respectively. Future work will entail realization of robust prototypes using embroidery of conductive E-threads straight upon the fabric, coating with breathable thermoplastic polyurethane to avoid moisture-trapping, simulations using realistically – shaped / sized tissue models, denser dipole placement to increase resolution, packaging/integration, and *in-vivo* validation. Applications envisioned include unobtrusive integration into baby cribs, children's bed sheets or rollable mats to provide early detection of length/height related disorders. This is a game-changing alternative to existing infantometer and measuring tape technologies that pose logistical challenges to patients, parents, and health care providers.

> REPLACE THIS LINE WITH YOUR PAPER IDENTIFICATION NUMBER (DOUBLE-CLICK HERE TO EDIT) <

7

ACKNOWLEDGMENT

The authors would like to thank Harsh Singhania (undergraduate student at Ohio State's ECE Dept.) for his assistance with the preliminary measurements of this work.

REFERENCES

- [1] P. Scherdel, J.-F. Salaün, M.-N. Robberecht-Riquet, L. Reali, G. Páll, E. Jäger-Roman, M. P. Crespo, M. Moretto, M. Seher-Zupančič, S. Agustsson, and M. Chalumeau, "Growth Monitoring: A Survey of Current Practices of Primary Care Paediatricians in Europe," *PLoS ONE*, vol. 8, no. 8, May 2013.
- [2] S. Carsley, C. S. Birken, K. Tu, E. Pullenayegum, and P. C. Parkin, "Examining growth monitoring practices for children in primary care," *Archives of Disease in Childhood*, 2017.
- [3] L. Säwendahl and M. L. Davenport, "Delayed diagnoses of Turner's syndrome: Proposed guidelines for change," *The Journal of Pediatrics*, vol. 137, no. 4, pp. 455–459, 2000.
- [4] M. Gasparetto, "Crohns disease and growth deficiency in children and adolescents," *World Journal of Gastroenterology*, vol. 20, no. 37, p. 13219, 2014.
- [5] D. Craig, D. Fayter, L. Stirr, and R. Crott, "Growth monitoring for short stature: update of a systematic review and economic model," *Health Technology Assessment*, vol. 15, no. 11, 2011.
- [6] C. R. Kahrs, M. C. Magnus, H. Stigum, K. E. A. Lundin, and K. Stordal, "Early growth in children with coeliac disease: a cohort study," *Archives of Disease in Childhood*, vol. 102, no. 11, pp. 1037–1043, 2017.
- [7] "Recommendations for growth monitoring, and prevention and management of overweight and obesity in children and youth in primary care," *Canadian Medical Association Journal*, vol. 187, no. 6, pp. 411–421, 2015.
- [8] P. Mahachoklertwattana, C. Preeyasombat, L. Choubtum, and A. Sriphrapradang, "Final Height after Long-Term Growth Hormone Treatment in Thai Children with Turner Syndrome," *Hormone Research*, vol. 49, no. Suppl. 1, pp. 55–55, 1998.
- [9] G. C. A. Gascoin-Lachambre, R. Brauner, L. Duche, and M. Chalumeau, "Pituitary Stalk Interruption Syndrome: Diagnostic Delay and Sensitivity of the Auxological Criteria of the Growth Hormone Research Society," *PLoS ONE*, vol. 6, no. 1, 2011.
- [10] R. W. Holl, D. Kunze, H. Etzrodt, W. Teller, and E. Heinze, "Turner syndrome: Final height, glucose tolerance, bone density and psychosocial status in 25 adult patients," *European Journal of Pediatrics*, vol. 153, no. 1, pp. 11–16, 1994.
- [11] P. L. Selby, M. Davies, J. E. Adams, and E. B. Mawer, "Bone Loss in Celiac Disease Is Related to Secondary Hyperparathyroidism," *Journal of Bone and Mineral Research*, vol. 14, no. 4, pp. 652–657, Jan. 1999.
- [12] M. D. Onis, A. W. Onyango, J. V. D. Broeck, C. W. Chumlea, and R. Martorell, "Measurement and Standardization Protocols for Anthropometry Used in the Construction of a New International Growth Reference," *Food and Nutrition Bulletin*, vol. 25, 2004.
- [13] L. R. Braun and R. Marino, "Disorders of Growth and Stature," *Pediatrics in Review*, vol. 38, no. 7, pp. 293–304, 2017.
- [14] J. F. Hagan, J. S. Shaw, and P. M. Duncan, *Bright futures: guidelines for health supervision of infants, children, and adolescents*. Elk Grove Village, IL: Bright Futures/American Academy of Pediatrics, 2017.
- [15] R. J. Kuczmarski, *2000 CDC growth charts for the United States: methods and development*. Hyattsville, MD: Dept. of Health and Human Services, Centers for Disease Control and Prevention, National Center for Health Statistics, 2002.
- [16] D. Giovenale, C. Meazza, G. M. Cardinale, M. Sposito, C. Mastrangelo, B. Messini, G. Citro, M. Delvecchio, S. D. Maio, and M. Bozzola, "The Prevalence of Growth Hormone Deficiency and Celiac Disease in Short Children," *Clinical Medicine & Research*, vol. 4, no. 3, pp. 180–183, Jan. 2006.
- [17] "Well-Child Visits," *Well-Child Visits, Child Health USA 2014*, 10-Aug-2014. [Online]. Available: <https://mchb.hrsa.gov/chusa14/health-services-financing-utilization/well-child-visits.html>. [Accessed: 30-Nov-2017].
- [18] U. Sankilampi, A. Saari, T. Laine, P. J. Miettinen, and L. Dunkel, "Use of Electronic Health Records for Automated Screening of Growth Disorders in Primary Care," *Jama*, vol. 310, no. 10, p. 1071, Nov. 2013.
- [19] A. Islam, A. Kiourti, and J.L. Volakis, "A Microwave Tomographic Technique to Enhance Real-Imaginary Permittivity Image Quality," *2017 IEEE International Symposium on Antennas and Propagation*, San Diego, CA, Jul. 09 – Jul. 15, 2017.
- [20] S. Salman, A. Kiourti, and J.L. Volakis, "Rudimentary Deep Tissue Imaging Through a Wearable Real-Time Monitoring System," *2015 IEEE International Symposium on Antennas and Propagation*, Vancouver, Canada, Jul. 19–25, 2015.
- [21] L. D. Howe, K. Tilling, and D. A. Lawlor, "Accuracy of height and weight data from child health records," *Journal of Epidemiology & Community Health*, vol. 63, no. Suppl 2, pp. 79–79, Sep. 2009.
- [22] J. Thuéry and E. H. Grant, *Microwaves: industrial, scientific, and medical applications*. Boston: Artech House, 1992.
- [23] K. Chan, R. Cleveland, D. Means, "Evaluating compliance with FCC guidelines for human exposure to radiofrequency electromagnetic fields," *OET Bulletin 65*, vol. Supplement C, pp. 97-01, 1997.
- [24] C. H. Durney and D. A. Christensen, *Basic introduction to electromagnetics*. Boca Raton: CRC Press, 2000.
- [25] C. W. L. Lee, A. Kiourti, J. Chae, and J. L. Volakis, "A high-sensitivity fully-passive wireless neurosensing system for unobtrusive brain signal monitoring," *2015 IEEE MTT-International Microwave Symposium*, 2015.
- [26] A. Kiourti and J. L. Volakis, "Stretchable and Flexible E-Fiber Wire Antennas Embedded in Polymer," *IEEE Antennas and Wireless Propagation Letters*, vol. 13, pp. 1381–1384, 2014.
- [27] A. Kiourti and J. Volakis, "Colorful Textile Antennas Integrated into Embroidered Logos," *Journal of Sensor and Actuator Networks*, vol. 4, no. 4, pp. 371–377, Aug. 2015.
- [28] J. Zhong, A. Kiourti, T. Sebastian, Y. Bayram, and J. L. Volakis, "Conformal Load-Bearing Spiral Antenna on Conductive Textile Threads," *IEEE Antennas and Wireless Propagation Letters*, vol. 16, pp. 230–233, 2017.
- [29] A. Kiourti, C. Lee, and J. L. Volakis, "Fabrication of Textile Antennas and Circuits With 0.1 mm Precision," *IEEE Antennas and Wireless Propagation Letters*, vol. 15, pp. 151–153, 2016.
- [30] M. L. Scarpello, I. Kazani, C. Hertleer, H. Rogier, and D. V. Ginste, "Stability and Efficiency of Screen-Printed Wearable and Washable Antennas," *IEEE Antennas and Wireless Propagation Letters*, vol. 11, pp. 838–841, 2012.
- [31] A. Kazmi, M. Rizwan, L. Sydanheimo, L. Ukkonen, and J. Virkki, "A reliability study of coating materials for brush-painted washable textile RFID tags," *2016 6th Electronic System-Integration Technology Conference (ESTC)*, 2016.
- [32] C. Hertleer, A. V. Laere, H. Rogier, and L. V. Langenhove, "Influence of Relative Humidity on Textile Antenna Performance," *Textile Research Journal*, vol. 80, no. 2, pp. 177–183, 2009.
- [33] X. Jia, A. Tennant, R. Langley, W. Hurley, and T. Dias, "Moisture effects on a knitted waveguide," *2016 Loughborough Antennas & Propagation Conference (LAPC)*, 2016.
- [34] J. Kim and Y. Rahmat-Samii, "Implanted Antennas Inside a Human Body: Simulations, Designs, and Characterizations," *IEEE Transactions on Microwave Theory and Techniques*, vol. 52, no. 8, pp. 1934–1943, 2004.
- [35] T. K. McNerny, "Reassessment of exposure to radiofrequency electro-magnetic fields limits and policies," *Federal Register*, vol. 78, no. 107, pp. 33654–33687, Jun. 2013.
- [36] U.S. Government Accountability Office. Telecommunications: Exposure and Testing Requirements for Mobile Phones Should be Reassessed. [Online]. Available: <http://www.gao.gov/products/GAO-12-771>, accessed Sep. 8, 2015.
- [37] M. Martínez-Bürdalo, A. Martín, M. Anguiano, and R. Villar, "Comparison of FDTD-calculated specific absorption rate in adults and children when using a mobile phone at 900 and 1800 MHz," *Physics in Medicine and Biology*, vol. 49, no. 2, pp. 345–354, May 2004.

- [38] R. D. Morris, L. L. Morgan, and D. Davis, "Children Absorb Higher Doses of Radio Frequency Electromagnetic Radiation From Mobile Phones Than Adults," *IEEE Access*, vol. 3, pp. 2379–2387, 2015.



Keren Zhu received the B.S. degree in electrical and computer engineering from The Ohio State University, Columbus, OH, USA, in 2017 and is currently working toward the Master degree in electrical and computer engineering at The Ohio State University.

She is currently a student research assistant at ElectroScience Laboratory, Columbus, OH, USA. From May 2016 to July 2016, she was a student intern at Hangzhou TuoXing Electronic Tech Co., Hangzhou, China. Her main research interests include electromagnetics, antennas and RF circuits.



Lisa Militello completed her undergraduate in nursing from the University of Pittsburgh, PA (1999). She completed concurrent Masters degrees in public health and nursing from the University of Pittsburgh, PA (2001). She received a PhD in healthcare innovation from Arizona State University, Phoenix, AZ (2014). She served as a Post-Doctoral Research Fellow from 2014-2016 at The Ohio State

University, Columbus, OH.

She is currently an Assistant Professor in the College of Nursing at The Ohio State University, Columbus, OH. She is a Board Certified Pediatric Nurse Practitioner. She has over 15 years experience working in pediatric clinical care. She was competitively selected for fellowship to Health 2.0 TECHquality (2017-2018), Health Data Exploration Summer Institute (2017), and mHealth Training Institute (2016). She has over 30 peer-review publications/presentations. Her research interests focus on the merger of technology with behavior change strategies and adaptive research methods to promote family health and wellness.



Asimina Kiourti (S'10–M'14) received the Diploma degree in electrical and computer engineering from the University of Patras, Patras, Greece, in 2008, the M.Sc. degree in technologies for broadband communications from University College London, London, U.K., in 2009, and the Ph.D. degree in electrical and computer engineering from the National Technical University of Athens, Athens,

Greece, in 2013.

She is currently an Assistant Professor of Electrical and Computer Engineering at The Ohio State University and the ElectroScience Laboratory, Columbus, OH, USA. From 2013 to 2016 she served as a Post-Doctoral Researcher and then a Senior Research Associate at the ElectroScience Laboratory. To date, she has (co-)authored over 37 journal papers, 85 conference papers, and 7 book chapters. Her research interests include wearable and implantable sensors, antennas and electromagnetics for body area applications, and flexible textile-based electronics.

Dr. Kiourti has received several awards and scholarships, including the IEEE Engineering in Medicine and Biology Society (EMB-S) Young Investigator Award for 2014, the IEEE Microwave Theory and Techniques Society (MTTS) Graduate Fellowship for Medical Applications for 2012, and the IEEE Antennas and Propagation Society (AP-S) Doctoral Research Award for 2011. She is currently serving as an Associate Editor for the IEEE Transactions on Antennas and Propagation.